



The mobility and fate of Cr during aging of ferrihydrite and ferrihydrite organominerals



Yao Zhao ^{a,b}, Alba Otero-Fariña ^b, Ke-Qing Xiao ^{b,*}, Oliver W. Moore ^b, Steven A. Banwart ^b, Fu-Jun Ma ^a, Qing-Bao Gu ^a, Caroline L. Peacock ^b

^aState Key Laboratory of Environmental Criteria and Risk Assessment, Chinese Research Academy of Environmental Sciences, Beijing 100012, China

^bSchool of Earth & Environment, University of Leeds, Leeds, LS2 9JT, UK

ARTICLE INFO

Article history:

Received 17 August 2022

Accepted 25 February 2023

Available online 1 March 2023

Associate editor: Owen Duckworth

Keywords:

Cr(VI)
Chromium
Chromate
Iron (oxyhydr)oxides
Iron (hydr)oxides
Fe minerals
Organic carbon
Carboxyl
Binding strength
Aging
Mobility
Retention

ABSTRACT

The fixation of environmentally hazardous Cr(VI) in soils is largely attributed to its retention by iron (Fe) (oxyhydr)oxides in the soil environment, which are prevailingly associated with organic carbon (OC). The effect of OC with different binding strengths on Cr(VI) adsorption and the mobility and fate of Cr(VI) during aging of Fe (oxyhydr)oxide however, are unknown. Here we investigate how OC binding strength influences Cr(VI) adsorption to ferrihydrite (Fh) organominerals, the aging of Fh organominerals and the subsequent retention or release of Cr(VI) as aging proceeds. We conduct Cr(VI) adsorption experiments onto Fh organominerals, apply surface complexation modelling to study the relative binding strengths between OC and Cr(VI), and then conduct aging experiments to track the redistribution of Cr(VI). We show based on the relative binding strength between OC and Cr(VI), that weakly-bound OC at different C loadings has almost no discernable influence on Cr(VI) adsorption, while strongly-bound OC significantly suppresses Cr(VI) adsorption via surface site blocking and/or electrostatic repulsion. The mobility and fate of Cr(VI) with Fh organominerals during the aging process is strongly influenced by the presence of OC. Weakly-bound carboxyl-poor OC not only near doubles the rate of Cr(VI) retained (i.e., Cr(VI) redistribution from a weakly-bound to a strongly-bound fraction) in neoformed Fe minerals at pH 5.0, but also increases the final proportion of Cr(VI)_{strongly-bound}, which we attribute to the loose and porous structure of Fh organominerals and easier replacement of weakly-bound OC by Cr(VI). More strongly-bound carboxyl-rich OC and higher pH however, reduces the influence of OC, such that the rate of Cr(VI) retained is similar to or lower than that for the pure Fh system, which we attribute to the fact that the strongly-bound OC is less easily replaced by Cr(VI) and hence Cr(VI) is less able to access surface sites or surface pores and thus to be retained inside neoformed minerals. Overall we suggest that OC with higher carboxyl-richness will further suppress the rate of Cr(VI) retained and overall proportion of Cr(VI)_{strongly-bound}, and thus that the mobility and fate of Cr(VI) in soils is strongly controlled by the carboxyl-richness of OC in Fe organominerals.

© 2023 The Author(s). Published by Elsevier Ltd. This is an open access article under the CC BY license (<http://creativecommons.org/licenses/by/4.0/>).

1. Introduction

Chromium, especially hexavalent chromium, can be released into the environment from a variety of industrial sources, like leather processing and finishing, steel processing, ceramic processing, electroplating, catalytic manufacture and drilling muds (Barnhart, 1997; Darrie, 2001; Jacobs and Testa, 2005). Hexavalent chromium Cr(VI) is the most common Cr species, is highly toxic and also more soluble and bioavailable than trivalent chromium Cr(III), and thus presents a mobile biohazard in aquatic and soil

ecosystems (Chandra and Kulshreshtha, 2004; Costa, 1997; Shanker et al., 2005). The potential environmental harm posed by Cr(VI) means that it is important to understand how this species interacts with soil constituents in order to predict Cr mobility and fate, and to develop soil remediation methods.

Compared to other soil minerals, Fe (oxyhydr)oxides, especially ferrihydrite (Fh), have widespread occurrence, high specific surface area and various binding sites for adsorption of solution species (Hiemstra, 2013; Larsen and Postma, 2001; Michel et al., 2007). As such they act as efficient adsorbents of organics (Cornell and Schwertmann, 2003) and heavy metal contaminants including Cr(VI) in soils (Gu et al., 2017; Mikutta et al., 2014). To gain insight into the mechanisms of Cr(VI) fixation in natural soil environments, Cr(VI) adsorption behavior to Fh is extensively investigated

* Corresponding author.

E-mail address: k.q.xiao@leeds.ac.uk (K.-Q. Xiao).

(Ding et al., 2018; Hajji et al., 2019; Johnston and Chrysochoou, 2012, 2016; Veselská et al., 2016; Whitaker et al., 2018). At the macroscopic level, Cr(VI) adsorption onto Fh exhibits a typical anion adsorption edge, with adsorption decreasing with increasing pH (Veselská et al., 2016). Adsorption edges show no significant difference with changes in Cr(VI) concentration and adsorbate/adsorbent ratio (Cr(VI) concentrations of 10^{-6} , 10^{-5} , 10^{-4} M) or ionic strength (0.001, 0.01, 0.1 M KNO_3) (Veselská et al., 2016). At the microscopic level, Cr(VI) tends to form inner-sphere bidentate complexes at high surface coverage and monodentate complexes at lower surface coverage on Fe minerals including Fh, goethite (Gt) and hematite (Hm), confirmed by spectroscopic techniques coupled with surface complexation modelling (Fendorf et al., 1997; Johnston and Chrysochoou, 2012, 2014; Veselská et al., 2016; Xie et al., 2015). Monodentate complexes may be the precursor of bidentate complexes (Grossl et al., 1997) and are particularly susceptible to ionic strength effects (Johnston and Chrysochoou, 2012, 2014; Xie et al., 2015). It is also reported that Al substitution in Fh disproportionately suppresses bidentate complexes over monodentate complexes (Johnston and Chrysochoou, 2016).

Authigenic Fh is metastable under oxic conditions however, and ages to more crystalline Fe minerals, like Gt and Hm (Das et al., 2011). Because aging involves dissolution, precipitation, aggregation, adsorption and desorption (Sakakibara et al., 2019) and the more crystalline Fe minerals also have different physical and chemical properties compared to Fh (Cornell and Schwertmann, 2003), the aging of Fe (oxyhydr)oxide can influence the mobility of adsorbed heavy metals (Francisco et al., 2018; Hu et al., 2020; Hu et al., 2018; Sakakibara et al., 2019). In addition Fh formed in natural environments is typically associated with organic carbon (OC) as a dominant reactive pool of carbon to form organominerals through a variety of sequestration processes that remove OC from solution to the solid mineral particles (Sposito, 2008). The interaction of OC with Fh is known in some cases to substantially effect the adsorption of the generally lower mass amounts of trace elements, such as Cr(VI) (Yu et al., 2020), in soil environments by blocking mineral surface sites (Chen et al., 2014; Field et al., 2019; Shimizu et al., 2013), which may further influence the redistribution of Cr(VI) during the aging process of Fh organominerals.

A limited number of studies focus on the mobility of Cr during aging of Fe (oxyhydr)oxides. The aging of pure Fh to more crystalline Fe minerals can increase the proportion of strongly-bound Cr(VI) (Yu et al., 2020; Yu et al., 2021; Zhu et al., 2019), decreasing the mobility of Cr(VI). On the other hand, aging of pure Fh also increases aqueous Cr(VI) at pH 7.5 (Zhu et al., 2019), increasing the mobility of Cr(VI). Different additives in the adsorption systems also have different influence on the distribution of Cr(VI) between strongly-bound and weakly-bound fractions. The presence of silicate in Fh-Si-Cr coprecipitates significantly decreases the proportion of strongly-bound Cr(VI) (Zhu et al., 2019), while the addition of citrate in solution also decreases strongly-bound Cr(VI) during aging at pH 5.0 but increases aqueous Cr(VI) during aging at pH 7.0 (Yu et al., 2021). To the authors' knowledge however, only one study investigates the influence of OC on the distribution of Cr during re-crystallisation of Fh in organominerals to other more crystalline Fe minerals, where it is observed that the aging of Fh-humic acid composites increases strongly-bound Cr after aging, probably via a redox reaction which reduces more soluble Cr(VI) to less soluble Cr(III) (Yu et al., 2020). Similarly rare are studies that reveal the microscopic mechanistic interactions between Fh organominerals and Cr(VI), in which the focus is not on the redox reduction of Cr(VI). Early work reveals a competitive adsorption between oxalate and Cr(VI), and emphasises the importance of the relative adsorption affinity of Cr(VI) and OC to Fe (oxyhydr)oxides (Mesuere and Fish, 1992a,b). The influence of OC on Cr(VI) adsorption behaviour to Fh organominerals, and the mobility

and fate of Cr(VI) during aging of these organominerals however, is still largely unknown.

One of the most important types of OC for Fe (oxyhydr)oxide-OC associations is carboxyl-rich OC. Carboxyl functional groups are prevalent in natural OC (Rothe et al., 2000) and are highly reactive towards different mineral surfaces and metal ions (Rowley et al., 2017). Carboxyl-rich OC has a high adsorption affinity with Fe (oxyhydr)oxides during both its adsorption to preformed Fe (oxyhydr)oxides and during its coprecipitation with Fe (oxyhydr)oxides (Curti et al., 2021; Gu et al., 1995; Zhao et al., 2022), where OC is mostly adsorbed at mineral particle surfaces with a lesser amount incorporated into OC-Fe macromolecules and particle interiors (Chen et al., 2014; Curti et al., 2021; Eusterhues et al., 2011; Lehmann et al., 2008; Zhao et al., 2022). In addition, spectroscopic studies using Fourier-transform infrared (FTIR) spectroscopy and near edge X-ray absorption fine structure (NEXAFS) spectroscopy provide direct evidence for inner-sphere adsorption complexation between carboxyl functional groups and Fe (oxyhydr)oxides (Chen et al., 2014; Lv et al., 2016; Solomon et al., 2005). Thus OC in Fh organominerals is a potential competitor with Cr(VI) for adsorption sites.

Our recent studies document that carboxyl-richness in OC moieties plays an important role in controlling the affinity of OC to Fe minerals and influencing the properties of Fe minerals formed after aging. Our recent NEXAFS spectroscopy and surface complexation modelling show that as the number of carboxyl functional groups present in simple carboxylic OC compounds increases, the number of carboxylate-Fe bonds formed between carboxyl functional groups and the Fe particles increases, and thus the binding strength and stability of the OC associated with Fh also increases (Curti et al., 2021; Zhao et al., 2022). The presence of OC also substantially retards the aging of Fh to form more crystalline Fe minerals and this retardation increases with increasing OC binding strength (Zhao et al., 2022). Besides, the specific surface area (SSA) of Fe minerals after aging generally decreases compared to freshly synthesised Fh or Fh organominerals, whilst the specific surface area (SSA) and total pore volume (TPV) of Fe minerals after aging show an increasing trend with increasing OC binding strength (Zhao et al., 2022). The known behaviour of OC during organomineral formation, reactivity and aging is likely to have an important influence on Cr(VI) retention in soils.

Here we investigate how OC binding strength influences Cr(VI) adsorption to Fh organomineral coprecipitates, and the retention or release of Cr(VI) with the aging of Fh organominerals. We focus on the effect of carboxyl-rich OC and use simple mono-, di- and tri-carboxylic acids, possessing increasing carboxyl-richness and thus increasing binding strengths to the Fh organomineral coprecipitate particles. We perform Cr(VI) adsorption experiments with pure Fh and Fh-OC organomineral coprecipitates to observe the influence of OC binding strength on Cr adsorption. We then subject our Fh organomineral coprecipitates to aging experiments at 75 °C to observe how OC binding strength influences the distribution of Cr(VI) during the aging process. Our primary objectives are to (1) investigate the influence of carboxyl-rich OC with different binding strengths on Cr(VI) adsorption to Fh organominerals; (2) investigate the influence of carboxyl-rich OC with different binding strengths on the mobility and fate of Cr(VI) during aging of Fh organominerals; and (3) provide novel information for predicting the behaviour of Cr(VI) in contaminated soils.

2. Materials and methods

2.1. Preparation of Fh and Fh organomineral coprecipitates

Pure ferrihydrite (Fh) was prepared following the method of Schwertmann and Cornell (2000) for the precipitation of 2-line ferrihydrite via hydrolysis of Fe(III) salt solution. Briefly, Fh was

prepared by rapid hydrolysis of 0.1 M $\text{Fe}(\text{NO}_3)_3 \cdot 9\text{H}_2\text{O}$ (aq) with 1 M KOH at pH 7. Fh was washed several times over a week in equivalent volumes of 18.2 M Ω -cm MilliQ water, after which Fh was stored as a slurry at 4 °C (Schwertmann and Cornell, 2000). The mineralogy of the Fh was confirmed on freeze-dried subsamples via X-ray diffraction (XRD) using a Bruker D8 Diffractometer with Cu-K α radiation ($\lambda \approx 0.154$ nm). Diffractograms were recorded from 2 to 90°2 θ with 0.02°2 θ step size and 930 ms acquisition time. Silicon dioxide was used as an analytical standard. The specific surface area (SSA) of the Fh was determined by the multi-point BET (Brunauer, Emmett and Teller) technique using a Micromeritics Gemini VII Surface Area Analyser, with samples dried and degassed at room temperature for 24 h using N_2 (g) (<1 ppm CO_2 (g)) prior to analysis. All SSA analyses were performed in triplicate.

Fourteen Fh-OC organomineral coprecipitates with different wt% C were prepared with three simple carboxylic acids, which are prevalent in soil and sediment porewaters (Barcelona, 1980; Jones, 1998), following the method of Curti et al. (2021). The acids were denoted as acid n/m , where acid refers to the first three letters of the acid IUPAC name and n/m denotes the number of carboxyl groups (n) and the number of total carbon atoms (m). The acids used were pentanoic acid (Pen1/5), hexanedioic acid (Hex2/6) and butane 1, 2, 4 tricarboxylic acid (But3/7), which have one, two and three carboxyl functional groups, respectively. Briefly, 0.1 M $\text{Fe}(\text{NO}_3)_3 \cdot 9\text{H}_2\text{O}$ (aq) solutions were mixed with varied amounts of organic acids and then the pH values of the solutions were adjusted to ~ 7 with 1 M KOH, whereupon the acids coprecipitated with the Fh, forming Fh organomineral coprecipitates with different wt% C. Fh organomineral coprecipitates were washed several times over a week with 18.2 M Ω -cm MilliQ water, after which coprecipitates were stored as a slurry at 4 °C, and part of the coprecipitates were freeze-dried for further analysis. The amounts of organic acids associated with solid minerals were varied taking into account the solubility of the acids in solution and their affinity for Fh during coprecipitation. For Pen1/5 solubility and affinity are low and constrain the maximum carbon sequestration to a low level, while for Hex2/6 and But3/7 affinity is higher and allows a maximum sequestration of at least ~ 7 wt%C (Curti et al., 2021; Zhao et al., 2022).

The mineralogy of the Fh coprecipitates was confirmed on freeze-dried subsamples via XRD as described above. The C contents of the solids were determined on freeze-dried subsamples using a LECO SC-144DR Dual Range Sulphur and Carbon Analyzer. The Fe contents of the solids were determined after total digestion using 6 M HCl using an Atomic Absorption Spectrophotometer (iCE 3300 AAS). Fourteen coprecipitates were obtained as shown in Table 1. Plastic labware and AR grade reagents were used throughout all the preparations.

Table 1
Fh organominerals synthesised.

Name	Number of carboxyl groups in organic acids	C:Fe molar ratio	wt%C
Fh_Pen1/5_1.2 wt%C	1	0.098	1.2
Fh_Pen1/5_1.9 wt%C	1	0.157	1.9
Fh_Hex2/6_2.9 wt%C	2	0.246	2.9
Fh_Hex2/6_3.3 wt%C	2	0.283	3.3
Fh_Hex2/6_4.1 wt%C	2	0.358	4.1
Fh_Hex2/6_4.5 wt%C	2	0.396	4.5
Fh_Hex2/6_6.4 wt%C	2	0.588	6.4
Fh_Hex2/6_7.0 wt%C	2	0.652	7.0
Fh_But3/7_5.1 wt%C	3	0.461	5.1
Fh_But3/7_6.0 wt%C	3	0.555	6.0
Fh_But3/7_6.6 wt%C	3	0.620	6.6
Fh_But3/7_7.3 wt%C	3	0.699	7.3
Fh_But3/7_7.8 wt%C	3	0.757	7.8
Fh_But3/7_10.2 wt%C	3	1.060	10.2

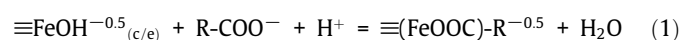
2.2. Adsorption of Cr(VI) on Fh and Fh organomineral coprecipitates and surface complexation modelling

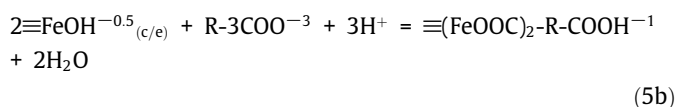
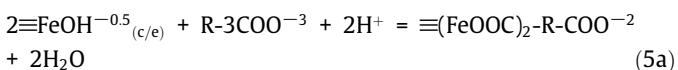
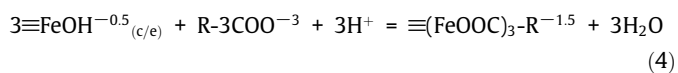
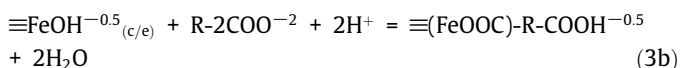
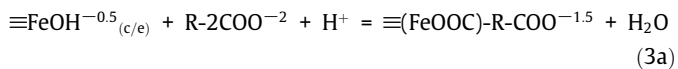
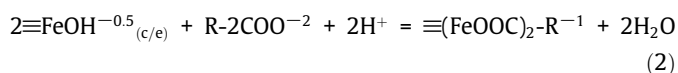
2.2.1. Adsorption of Cr(VI) on Fh and Fh organomineral coprecipitates

The Cr(VI) adsorption experiments onto Fh and Fh organomineral coprecipitates were conducted following (Moon and Peacock, 2012, 2013). Batch adsorption pH edge experiments of Cr(VI) adsorbed on Fh or Fh organomineral coprecipitates were prepared from pH 3.5 to pH 10.0. The Fh or Fh organomineral slurry was added into MilliQ water and Cr(VI) stock solution was added to give a total volume of 30 mL, a solid solution ratio of 1 g dry sorbent L^{-1} and total Cr(VI) concentrations of 1.92×10^{-6} , 1.92×10^{-5} , 1.92×10^{-4} M (0.01 wt%, 0.1 wt% and 1.0 wt% Cr at 100% adsorption, respectively) for Fh and 1.92×10^{-5} M (0.1 wt% Cr at 100% adsorption) for Fh organomineral coprecipitates, in 0.1 M NaNO_3 background electrolyte. After addition of stock solution, pH of the resulting suspensions was adjusted by dropwise addition of either dilute HNO_3 or NaOH . After shaking continuously for 48 h to ensure adsorption equilibrium (Zhu et al., 2010), the suspensions were centrifuged at 2250 g for 15 min to obtain a clear supernatant for determination of Cr(VI) concentration. Supernatants were filtered using 0.2 μm polycarbonate membrane filters and acidified with 2% HNO_3 for aqueous Cr(VI) analysis by inductively coupled plasma mass spectrometry (ICP-MS). All the adsorption experiments were performed in duplicate. Experimental solution speciation of Cr(VI) was calculated as a function of pH using PHREEQC (Parkhurst and Appelo, 1999) and the MINTEQA4 database (Charlton and Parkhurst, 2002).

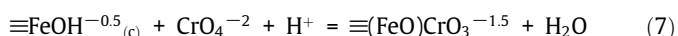
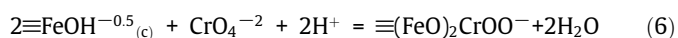
2.2.2. Surface complexation modelling

In previous work a surface complexation modelling approach is successfully used to simulate the adsorption of simple organic acids on preformed Gt (Evanko and Dzombak, 1999; Mesuere and Fish, 1992a,b) and the adsorption of Pen1/5, Hex2/6 and But3/7 to pure Fh (Zhao et al., 2022). In our previous work we show that for the same Fh_Pen1/5, Fh_Hex2/6 and Fh_But3/7 organominerals as used here, with equivalent C loadings (up to ~ 10 wt% C), OC is mainly adsorbed at the Fh particle surfaces via carboxylate-Fe complexation involving ligand exchange between $-\text{COOH}$ functional groups and $-\text{FeOH}$ sites. As such we represent OC adsorption according to our previous work in which we constrain the surface complexation reactions for the adsorption of OC on Fh_Pen1/5, Fh_Hex2/6 and Fh_But3/7 (Zhao et al., 2022). For Pen1/5 we find OC adsorption via one carboxyl group in a single-bonded monodentate configuration occurring on both $-\text{FeOH}$ edge and corner surface sites, represented by reaction (1). For Hex2/6, we find OC adsorption via two carboxyl groups in a bidentate mononuclear or bidentate binuclear configuration occurring on both the $-\text{FeOH}$ edge and corner surface sites, represented by reaction (2). We also find OC adsorption via one carboxyl group in a monodentate mononuclear configuration occurring on both $-\text{FeOH}$ edge and corner surface sites, in which the non-bonding carboxyl group is deprotonated at higher pH ($> \text{pH} \sim 5.5$) and protonated at lower pH ($< \text{pH} \sim 5.5$), represented by reactions (3a) and (3b), respectively. Finally for But3/7 we find OC adsorption via three carboxyl groups in a tridentate trinuclear configuration occurring on both the $-\text{FeOH}$ edge and corner surface sites, represented by reaction (4). We also find adsorption via two carboxyl groups in a bidentate mononuclear or bidentate binuclear configuration occurring on both the $-\text{FeOH}$ edge and corner surface sites, in which the non-bonding carboxyl group is deprotonated at higher pH ($> \text{pH} \sim 4.5$) and protonated at lower pH ($< \text{pH} \sim 4.5$), represented by reactions (5a) and (5b), respectively:





A surface complexation modelling approach is also successfully used to simulate the adsorption of Cr(VI) onto Fe (oxyhydr)oxides (Bompoti et al., 2019; Veselská et al., 2016; Xie et al., 2015). The adsorption of Cr(VI) onto pure Fe (oxyhydr)oxides is reported to occur via inner-sphere complexation involving ligand exchange between the $\text{HCrO}_4^-/\text{CrO}_4^{2-}$ oxyanion and Fe (oxyhydr)oxide $-\text{FeOH}$ surface adsorption sites (Fendorf et al., 1997; Johnston and Chrysochoou, 2012, 2014). Recent spectroscopic work further finds that Cr(VI) adsorbs onto corner-sharing Fe (oxyhydr)oxide $-\text{FeOH}$ sites as non-protonated monodentate and bidentate complexes and successfully models this adsorption with a surface complexation model that considers the formation of these species at the mineral surfaces (Johnston and Chrysochoou, 2014). As such we represent Cr(VI) adsorption on Fh using CrO_4^{2-} as the primary reactive chromate species, which adsorbs to corner-sharing $-\text{FeOH}$ sites ($\equiv\text{FeOH}_c^{-0.5}$) via bidentate (reaction (6)) and monodentate (reaction (7)) surface complexes:



The basic Stern model (BSM) (Westall and Hohl, 1980) was used to account for the surface electrostatics in the Fh and Fh organomineral coprecipitate systems (Moon and Peacock, 2013; Otero-Fariña et al., 2017; Zhao et al., 2022) with a 3-site 1 pK formalism for protonation of the Fh surface, involving two types of singly-coordinated surface oxygens (edge-sharing $\equiv\text{FeOH}_e^{-0.5}$ and corner-sharing $\equiv\text{FeOH}_c^{-0.5}$) and the triply-coordinated oxygens ($\equiv\text{Fe}_3\text{O}^{-0.5}$) (Hiemstra and Van Riemsdijk, 2009; Hiemstra et al., 1989; Hiemstra et al., 1996). The model input parameters for the binding constants for protonation of the surface functional groups, binding constants for electrolyte ions associating with these groups and capacitance of the Stern layer were fixed at those used in previous work with Fh and Fh organomineral coprecipitates (Moon and Peacock, 2013; Otero-Fariña et al., 2017). The SSA of the Fh was fixed to the BET measurement while the SSA of the Fh organominerals was estimated from calculation using the SSA of the Fh weighted to the mineral:OC mass ratio of each organomineral. The surface site densities of the Fh were fixed to those measured in previous work (Moon and Peacock, 2013; Otero-Fariña et al., 2017) while the surface site densities of the Fh organominerals were estimated from calculation using the surface site densities of Fh weighted to the mineral:OC mass ratio of each organomineral.

Following these approaches, Cr(VI) adsorption onto Fh and both OC and Cr(VI) adsorption onto Fh organomineral coprecipitates was fit to a thermodynamic surface complexation model using the program EQLFOR (Sherman et al., 2008). For the Fh system, the adsorption experiment data for the adsorption of Cr(VI) to Fh was fitted. For the Fh organomineral coprecipitate system, OC and Cr(VI) adsorption was envisaged as a competition between Cr(VI) and OC for available adsorption sites on Fh. In this approach the binding constants for the adsorption of Pen1/5, Hex2/6 and But3/7 were initially fixed at those determined in the previous work for the adsorption of Pen1/5, Hex2/6 and But3/7 onto pure Fh (Zhao et al., 2022), while the binding constants for the adsorption of Cr(VI) were initially fixed to those determined for the pure Fh system. After reviewing the initial fits for the Cr(VI) adsorption onto the Fh organomineral coprecipitates, the final fits were improved with minor iteration of the end-member binding constants for OC adsorption, during which these binding constants changed by <0.9 log units compared to the initial end-member binding constants.

2.3. Aging of Cr(VI) adsorbed Fh and Fh organomineral coprecipitates

Aging experiments of Fh and Fh organomineral coprecipitates were conducted following the method of Zhao et al. (2022). Briefly, experiments were prepared by adding Fh or Fh organomineral coprecipitate slurry into MilliQ water and Cr(VI) stock solution was added to produce 2 g dry sorbent L^{-1} with 0.1 wt%Cr (Cr/Fe = 0.002), 1.1 wt%Cr (Cr/Fe = 0.02) and 5.4 wt%Cr (Cr/Fe = 0.10) at 100% adsorption for Fh, and 0.1 wt%Cr (Cr/Fe = 0.002) at 100% adsorption for Fh organomineral coprecipitates, in 0.01 M NaNO_3 background electrolyte. These suspensions were then adjusted to target pH values with dilute HNO_3 or NaOH . The pH values were buffered at pH 5 by adding 30 mM organic buffer 2-(N-Morpholino)ethane-sulphonic acid (MES) or pH 6.5 and 8 by adding 3-(N-Morpholino)propanesulphonic acid (MOPS). After shaking for 48 h to achieve adsorption equilibrium (Zhu et al., 2010), the resultant solutions were transferred to an electric oven kept at a temperature of 75 °C for up to 19 days. During aging, the vessels were gently shaken to keep the suspensions homogenised. Aliquots of the solid precipitates and solutions were collected and analysed at pre-designed time intervals to track changes in the physiochemical characteristics of the Fh coprecipitates (Section S2) and the redistribution of Cr(VI) as described below. At each sampling, pH measurements for pure Fh systems were conducted and recorded.

2.4. Redistribution of Cr(VI) during aging of pure Fh and Fh organomineral coprecipitates

To investigate the redistribution of Cr(VI) during aging of Fh and Fh organominerals, two 15-mL aliquots were subsampled from the reactor and either centrifuged (Fh system) or vacuum filtered (Fh organominerals) to separate solid minerals and supernatant or filtrate. The supernatant or filtrate were collected for measurement of aqueous Cr(VI) ($[\text{Cr}_{\text{aqueous}}]$). The remaining mineral particles were rinsed with 15 mL DI water, and re-suspended in 15 mL 0.1 M NaOH and shaken for 24 h to extract Cr(VI) following the method to extract As(V) from Fe (oxyhydr)oxides (Hu et al., 2020; Hu et al., 2018). Then resulting suspensions were filtered with 0.22 μm PES filters and the filtrate was collected for measurement of Cr(VI), which was operationally defined as weakly-bound Cr(VI) ($\text{Cr(VI)}_{\text{weakly-bound}}$). Proportions of Cr(VI) remaining in the solid, operationally defined as strongly-bound Cr(VI) ($\text{Cr(VI)}_{\text{strongly-bound}}$), were calculated based on mass balance. The Cr(VI) concentrations in all solutions generated above were measured by ICP-MS. All measurements were conducted at least in duplicate.

To better evaluate the influence of OC on the Cr(VI) redistribution from weakly-bound to strongly-bound fractions, the increasing proportions of Cr(VI)_{strongly-bound} (from 0 to ~80%) with aging time are fitted with the rate equation:

$$[A]_t = a + b \times t.$$

where $[A]_t$ is the fraction of Cr(VI)_{strongly-bound} at time t , a is intercept of the linear fit, and b is the slope of the linear fit, representing the rate of Cr(VI) retained.

3. Results

3.1. Adsorption of Cr(VI) to Fh and Fh organominerals

Experimental solution speciation at 1.92×10^{-6} , 1.92×10^{-5} , 1.92×10^{-4} M $[\text{Cr(VI)}]_{\text{total}}$ in 0.1 M NaNO_3 background electrolyte was calculated as a function of pH and shown in Fig. S1. Above pH 6.5, CrO_4^{2-} generally dominates, while below pH 6.5, HCrO_4^- dominates. In our adsorption experiments Cr(VI) therefore principally adsorbs as HCrO_4^- and CrO_4^{2-} .

The adsorption of Cr to Fh and Fh organominerals is plotted in Fig. 1 as a function of pH. In all cases Cr(VI) adsorption follows a reverse sigmoid adsorption edge, in which the amount of Cr(VI) adsorbed decreases as pH increases. For Fh_Pen1/5 and Fh_Hex2/6 organominerals, the presence of the organic acids at different loadings has almost no discernible influence on Cr(VI) adsorption. For Fh_But3/7 organominerals however, although Fh_But3/7_5.1 wt%C and Fh_But3/7_6.6 wt%C have lower or similar OC with respect to Fh_Hex2/6_6.4 wt%C, the adsorption edges are shifted to lower pH, which are increasingly shifted with increasing OC loading. The Fh_But3/7_10.2wt%C organomineral with the highest wt%C significantly suppresses the adsorption of Cr(VI), especially in the low pH regime.

3.2. Model fitting of Cr(VI) adsorption onto pure Fh and Fh organominerals

All model parameters are collected in Table 2, and the model fitting results for Cr(VI) adsorption on Fh and Fh organominerals are shown in Fig. 2. Our surface complexation model shows that Cr(VI) adsorbs to pure Fh and Fh organominerals predominantly via a bidentate surface complex at $\text{pH} < 5.5$ and a monodentate surface complex at $\text{pH} > 6.0$ (Fig. 2).

3.3. Redistribution of Cr(VI) during aging of Fh and Fh organominerals

For Fh the concentration of aqueous Cr(VI) increases with aging time, and this increase is more pronounced with increasing Cr(VI) concentrations and pH (Fig. 3). The Cr(VI) associated with the solid minerals exists as Cr(VI)_{strongly-bound} and Cr(VI)_{weakly-bound} species. The Cr(VI)_{strongly-bound} increases with aging time at the expense of Cr(VI)_{weakly-bound} at pH 5.0 and pH 6.5. The final proportion of Cr(VI)_{strongly-bound} decreases with increasing Cr(VI) concentration and pH (Fig. 3).

For Fh organominerals the concentration of aqueous Cr(VI) is negligible for Fh_Pen1/5 and Fh_Hex2/6 coprecipitates during the whole aging time, but for Fh_But3/7 coprecipitates aqueous Cr(VI) initially increases and then decreases as aging proceeds, and the total aqueous Cr(VI) at any given time also increases with the C loading of the coprecipitates (Fig. 4). The final amount of Cr(VI)_{strongly-bound} after 19-days at pH 5 shows no significant difference for all Fh organominerals with around 95% Cr(VI)_{strongly-bound}, while at pH 6.5 follows the order Fh_Pen1/5 coprecipitate ~ Fh_Hex2/6 coprecipitates > Fh_But3/7 coprecipitates.

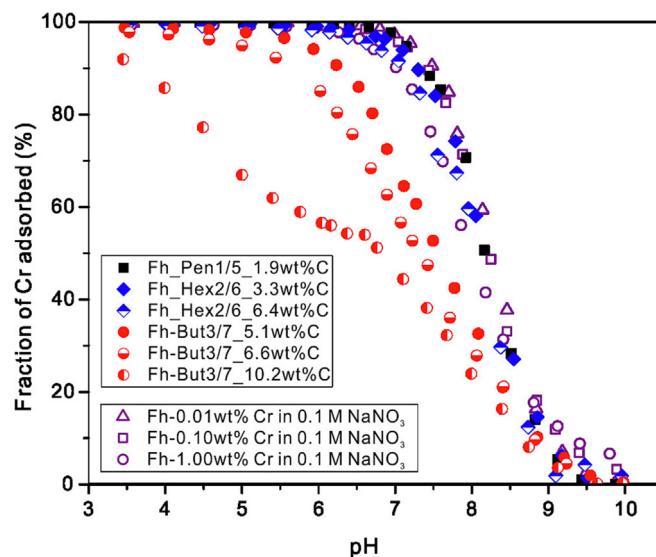


Fig. 1. Adsorption of Cr(VI) on Fh and Fh organominerals as a function of pH (3.5–10). Experiment conditions are 1.92×10^{-6} , 1.92×10^{-5} , 1.92×10^{-4} M $[\text{Cr(VI)}]_{\text{total}}$ for Fh (0.01 wt%, 0.1 wt% and 1.0 wt% Cr at 100% adsorption, respectively) and 1.92×10^{-5} M $[\text{Cr(VI)}]_{\text{total}}$ for Fh organominerals (0.1 wt% Cr at 100% adsorption), in 1 g sorbent L^{-1} in 0.1 M NaNO_3 background electrolyte. Pen1/5, Hex2/6 and But3/7 represent simple carboxyl-rich OC with one-, two- and three-carboxyl groups, respectively. The average error bar for duplicate experiments is smaller than the data points.

The fitting to increasing proportions of Cr(VI)_{strongly-bound} are shown in Fig. S5 and the rate data are presented in Table 3. The rate data shows that generally the presence of OC in the Fh organominerals increases the rate of Cr(VI) retained, compared to the Fh system. The positive influence of OC on Cr(VI) retained appears to decrease with increasing carboxyl-richness of OC in the sequestered acid molecules and generally follows the order Fh_Pen1/5 coprecipitate > Fh_Hex2/6 coprecipitates > Fh_But3/7 coprecipitates ~ pure Fh at pH 5.0. This trend is complicated by the commensurate increase in the C loading of the coprecipitates with increasing carboxyl-richness, but the Fh_Hex2/6_7.0wt%C and Fh_But3/7_7.3 wt%C have similar C loading, yet the latter has lower rates of Cr(VI) retained. The increasing pH condition further weakens the influence of OC, with rates of Cr(VI) retained following the order Fh_Pen1/5 coprecipitate > Fh_Hex2/6 coprecipitates ~ pure Fh > Fh_But3/7 coprecipitates at pH 6.5.

4. Discussion

4.1. Adsorption of Cr(VI) to Fh organominerals

4.1.1. Binding affinity of Cr(VI) and carboxyl-rich OC with Fh

The binding affinity of Cr(VI) and carboxyl-rich OC with Fh is quantified by conducting adsorption experiments and fitting these to a thermodynamic surface complexation model. Our surface complexation model shows that Cr(VI) adsorbs to pure Fh and Fh organominerals predominantly via a bidentate surface complex at $\text{pH} < 5.5$ and a monodentate surface complex at $\text{pH} > 6.0$ (Fig. 2), which are in agreement with spectroscopic work (Johnston and Chrysochoou, 2012, 2014). Thus, the overarching speciation of Cr(VI) is unaffected by the presence of OC. Our model fits for Fh and Fh organominerals also predict that the binding strength of the Cr(VI) complexes are the same in both systems, and the bidentate surface complex (Log K 19.25) is stronger than the monodentate surface complex (Log K 11.58), due to the formation of two chemical bonds, rather than a single chemical bond,

between the Cr(VI) species and the mineral surface (Grossl et al., 1997; Johnston and Chrysochoou, 2014). Our stability constants for the formation of the bidentate and monodentate surface complexes are consistent with the Cr(VI) stability constants reported in previous modelling studies for Cr(VI) adsorption on Fh (Bompoti et al., 2019; Veselská et al., 2016; Xie et al., 2015). Therefore the binding strengths of Cr(VI) complexes are also unaffected by the presence of OC. Overall our modelling shows that the binding strengths of our carboxylic OC and Cr(VI) complexes follow the order one-carboxyl binding (Log K's 9.2, 10.0/15.0) ~ monodentate Cr(VI) binding (Log K 11.58) < two-carboxyl binding (Log K 16.0, 19.70/24.0) ~ bidentate Cr(VI) binding (Log K 19.25) < three-carboxyl binding (Log K 27.2).

4.1.2. Influence of carboxyl-rich OC with different binding strengths on Cr(VI) adsorption to Fh organominerals

Despite the overarching speciation and binding strength of Cr(VI) complexes to Fh remaining unchanged by the presence of OC, the carboxyl-richness of the OC does have an effect on the adsorption behaviour of Cr(VI). For Fh_Pen1/5 and Fh_Hex2/6 organominerals, the presence of OC at different C loadings has almost no discernible influence on Cr(VI) adsorption (Fig. 1). For Fh_But3/7 organominerals however, although Fh_But3/7_5.1 wt% C and Fh_But3/7_6.6 wt% C have lower or similar OC compared to Fh_Hex2/6_6.4 wt% C, the adsorption edges and the equivalence point for bidentate and monodentate complexes are shifted to lower pH, which are increasingly shifted with increasing C loading (Fig. 2). The suppression of Cr(VI) adsorption for the Fh_But3/7 organominerals can be explained by several mechanisms. The first is the blocking of surface adsorption sites by the adsorbed organic acids on the minerals, such that the mineral adsorption capacity is reduced. Surface site blocking effects will vary, depending on the concentrations of the organic acids and Cr(VI), on their relative affinities competing for the mineral surface sites and on surface site concentration (Rai et al., 1986). Surface coverages of the mineral fraction of the different organominerals by organic acids and Cr(VI) are shown in Table 4. For But3/7 adsorbed via 2 or 3 of its available carboxyl groups, the surface coverage of the mineral exceeds 100% at the maximum C loadings, demonstrating that surface site blocking is potentially a factor in the suppression of Cr(VI) adsorption for the Fh_But3/7 composites. Interestingly the C loading for Fh_Hex2/6_6.4 wt% C is very similar to Fh_But3/7_6.6 wt% C, but no discernible inhibition of Cr(VI) adsorption is observed (Fig. 1). This suggests that Hex2/6 adsorbs predominantly via one-carboxyl adsorption in which the surface coverage is significantly lower than But3/7 adsorbing via two- or three- carboxyl adsorption (Table 4). This is in agreement with previous spectroscopic and modelling work suggesting that Hex2/6 adsorbs to Fh via one or two of its available carboxyl groups (Curti et al., 2021; Zhao et al., 2022).

Alternatively the monodentate Hex2/6 complex has a lower binding strength (Log K 10.0/15.0; Table 2) with Fh than the Cr(VI) bidentate complex (Log K 19.25; Table 2). The Cr(VI) may thus be able to better displace (out compete) Hex2/6 from the mineral surface. We suggest that higher concentrations of Hex2/6 are required to suppress Cr(VI) adsorption. Our hypothesis is supported by the report that much higher concentrations of weakly binding anions (in our case Hex2/6) are required to reduce adsorption of strongly binding anions (in our case Cr(VI)) (Mesuere and Fish, 1992b). The different surface coverages and binding strengths of OC also explain why But3/7 suppresses the formation of bidentate Cr(VI) but favours the formation of monodentate Cr(VI). The higher surface coverage by But3/7 likely results in a decreasing amount of surface sites available for the formation of bidentate Cr(VI) complexes, which require two surface sites, whilst the higher binding strength of But3/7 makes it more difficult for Cr

(VI) to replace OC and make sites available for the formation of bidentate Cr(VI) complexes. In addition, Fh coprecipitated with OC results in Fh with larger lattice spacings, fewer crystal planes, smaller particle diameters and more crystallographic defects (Eusterhues et al., 2014; Eusterhues et al., 2008), which possibly disproportionately decreases adjacent corner-sharing surface sites that are required for the formation of Cr(VI) bidentate complexes. By contrast, the formation of monodentate Cr(VI) complexes is relatively less influenced by the blocking of surface site or changes in surface site types, and as a result, monodentate Cr(VI) complexes are possibly favoured for the But3/7 organominerals.

Another mechanism that might explain the suppression of Cr(VI) adsorption for the Fh_But3/7 organominerals may be related to their spatial location on the surface of Fe (oxyhydr)oxide minerals. Previous work suggests that Pen1/5 and Hex2/6 adsorbed via monodentate complexes may adsorb perpendicular to the Fh surface, whilst But3/7 adsorbed by bidentate and/or tridentate complexes necessarily requires the acid molecules to align parallel with the Fh surface (Curti et al., 2021). Previous work also shows that competitive adsorption between FA and As(V) on goethite is much stronger than between HA and As(V) because the distribution of FA is closer to the goethite surface, leading to stronger electrostatic repulsion between adsorbed FA and adsorbing As(V) (Weng et al., 2009). As such if the parallel But3/7 is closer to the mineral surface than the perpendicular Pen1/5 and Hex2/6, then electrostatic repulsion between But3/7 and Cr(VI) will be stronger than that between Pen1/5/Hex2/6 and Cr(VI), and thus the suppression of Cr(VI) adsorption is likely enhanced.

4.2. Redistribution of Cr(VI) during aging of Fh and Fh organominerals

4.2.1. Redistribution of Cr(VI) in pure Fh systems

Aqueous Cr(VI) increases during aging of Fh (Fig. 3), likely because the Fe (oxyhydr)oxide becomes more compact with lower SSA and thus the adsorption capacity for Cr(VI) decreases as aging proceeds. As expected aqueous Cr(VI) concentrations are therefore higher for Fh systems that have higher Cr(VI) adsorbed (Fig. 3). Aqueous Cr(VI) concentrations are also higher for Fh aged under higher pH conditions (Fig. 3), likely because there are a greater proportion of deprotonated and thus negatively charged $-\text{FeOH}$ sites at higher pH, which electrostatically repel anionic Cr(VI) species.

As aging proceeds however, in addition to the loss of Cr(VI) to solution, the Cr(VI) that remains associated with the solid minerals also appears to transition from a weakly-bound to strongly-bound fraction (Fig. 3), which is also observed during aging of Cr(VI)-Fh coprecipitates (Sun et al., 2021; Zhu et al., 2019), suggesting that the affinity and thus the bonding environment of Cr(VI) changes during the aging process. Previous studies report that heavy metals like As(V) are converted from weakly-bound As(V) to strongly-bound As(V) during aging of Fh because As(V) species are incorporated into structural defects or surface pores of Fe minerals like lepidocrocite, hematite and magnetite, as observed by scanning transmission electron microscopy and extended X-ray absorption fine structure spectroscopy (Hu et al., 2020; Hu et al., 2018; Park et al., 2018; Wang et al., 2011). Like As(V) we therefore attribute our observed decrease in the fraction of $\text{Cr(VI)}_{\text{weakly-bound}}$ and concomitant increase in the fraction of $\text{Cr(VI)}_{\text{strongly-bound}}$ to a migration of $\text{Cr(VI)}_{\text{weakly-bound}}$, located on mineral surfaces, into structural defects and/or surface pores of Fe minerals formed after aging. During aging of Fe (oxyhydr)oxide in natural environments our results therefore indicate that some Cr(VI) becomes strongly-bound by transitioning from a surface bound to a structurally incorporated and thus more strongly bound complex, whilst some Cr(VI) is released into solution as aqueous Cr(VI).

It is noteworthy that in systems with 0.1 wt%Cr at 100% adsorption, all Cr(VI) remains associated with the minerals after 10 days

Table 2
Parameters for the surface complexation model for adsorption of Cr(VI) and carboxylic acids on Fh and Fh organominerals.

wt% C			Pure Fh	Fh organomineral						
				Pen1/5	Hex2/6	Hex2/6	But3/7	But3/7	But3/7	
				1.9 ^c	3.3 ^c	6.4 ^c	5.1 ^c	6.6 ^c	10.2 ^c	
Specific surface area (m ² /g)			300 ^a	290 ^d	280 ^d	261 ^d	265 ^d	255 ^d	230 ^d	
≡FeOH _e ^{-0.5} (mmol/g)			1.25 ^b	1.21 ^e	1.17 ^e	1.09 ^e	1.11 ^e	1.06 ^e	0.96 ^e	
≡FeOH _c ^{-0.5} (mmol/g)			1.74 ^b	1.68 ^e	1.62 ^e	1.51 ^e	1.54 ^e	1.48 ^e	1.34 ^e	
≡Fe ₃ O ^{-0.5} (mmol/g)			0.598 ^b	0.579 ^e	0.558 ^e	0.520 ^e	0.529 ^e	0.509 ^e	0.460 ^e	
C _{stern} (F/m ²)			1.10 ^b							
Log K _{FeOH(c)}	≡FeOH _(c) ^{-0.5} + H ⁺ = ≡FeOH _(c) ^{0.5}		7.99 ^b							
Log K _{FeOH(c)_Na}	≡FeOH _(c) ^{-0.5} + Na ⁺ = ≡FeOH _(c) ^{0.5} -Na ⁺		-1.00 ^b							
Log K _{FeOH2(c)_NO3}	≡FeOH _(c) ^{-0.5} + NO ₃ ⁻ = ≡FeOH _(c) ^{0.5} -NO ₃ ⁻		-1.00 ^b							
(where equations above are repeated for (≡FeOH _(e) ^{-0.5}))										
Log K _{Fe3O}	≡Fe ₃ O ^{-0.5} + H ⁺ = ≡Fe ₃ OH ^{0.5}		7.99 ^b							
Log K _{Fe3O_Na}	≡Fe ₃ O ^{-0.5} + Na ⁺ = ≡Fe ₃ O ^{-0.5} -Na ⁺		-1.00 ^b							
Log K _{Fe3OH_NO3}	≡Fe ₃ OH ^{0.5} + NO ₃ ⁻ = ≡Fe ₃ OH ^{0.5} -NO ₃ ⁻		-1.00 ^b							
		Log K ₁	Log K ₂	Log K ₃						
Pentanoic acid (Pen1/5)		4.84 ^f								
Hexanedioic acid (Hex2/6)		4.42 ^f	5.41 ^f							
Butane 1, 2, 4 tricarboxylic acid (But3/7)		4.31 ^g	4.82 ^g	5.21 ^g						
		Δz ₀	Δz ₁							
1. Log K _{FeOH(c)_Cr}	2≡FeOH _(c) ^{-0.5} + CrO ₄ ⁻² + 2H ⁺ = ≡(FeO) ₂ CrOO ⁻¹ + 2H ₂ O	+1.0 ^h	-1 ^h		19.25 ^h					
2. Log K _{FeOH(c)_Cr}	≡FeOH _(c) ^{-0.5} + CrO ₄ ⁻² + H ⁺ = ≡(FeO)CrO ₃ ^{-1.5} + H ₂ O	+0.5 ^h	-1.5 ^h		11.58 ^h					
3. Log K _{FeOH(c/e)_OOC-R}	≡FeOH _(c/e) ^{-0.5} + R-COO ⁻ + H ⁺ = ≡(FeOOC)-R ^{-0.5} + H ₂ O	+0.5 ^h	-0.5 ^h			9.2 ^h				
4. Log K _{FeOH(c/e)_OOC-R}	2≡FeOH _(c/e) ^{-0.5} + R-2COO ⁻² + 2H ⁺ = ≡(FeOOC) ₂ -R ⁻¹ + 2H ₂ O	+1.0 ^h	-1.0 ^h			16.0 ^h	16.0 ^h			
5a. Log K _{FeOH(c/e)_OOC-R}	≡FeOH _(c/e) ^{-0.5} + R-2COO ⁻² + H ⁺ = ≡(FeOOC)-R-COO ^{-1.5} + H ₂ O	+0.5 ^h	-0.5 ^h			10.0 ^h	10.0 ^h			
5b. Log K _{FeOH(c/e)_OOC-R}	≡FeOH _(c/e) ^{-0.5} + R-2COO ⁻² + 2H ⁺ = ≡(FeOOC)-R-COOH ^{-0.5} + 2H ₂ O	+0.5 ^h	-0.5 ^h			15.0 ^h	15.0 ^h			
6. Log K _{FeOH(c/e)_OOC-R}	3≡FeOH _(c/e) ^{-0.5} + R-3COO ⁻³ + 3H ⁺ = ≡(FeOOC) ₃ -R ^{-1.5} + 3H ₂ O	+1.95 ^h	-0.45 ^h					27.20 ^h	27.20 ^h	27.20 ^h
7a. Log K _{FeOH(c/e)_OOC-R}	2≡FeOH _(c/e) ^{-0.5} + R-3COO ⁻³ + 2H ⁺ = ≡(FeOOC) ₂ -R-COO ⁻² + 2H ₂ O	+1.3 ^h	-0.3 ^h					19.70 ^h	19.70 ^h	19.70 ^h
7b. Log K _{FeOH(c)_OOC-R}	2≡FeOH _(c) ^{-0.5} + R-3COO ⁻³ + 3H ⁺ = ≡(FeOOC) ₂ -R-COOH ⁻¹ + 2H ₂ O	+1.3 ^h	-0.3 ^h					24.00 ^h	24.00 ^h	24.00 ^h

^a Measured in this study.

^b From Moon and Peacock (2013) and Otero-Fariña et al. (2017).

^c Measured by LECO.

^d Estimated from calculation using the specific surface area of the pure Fh weighted to the mineral:OC mass ratio of each organomineral.

^e Estimated from calculation using the surface site densities of the pure Fh weighted to the mineral:OC mass ratio of each organomineral.

^f From Dean (1987).

^g Calculated using ACD/I-Lab 2.0 (ACD/I-Lab, version 2.0, Advanced Chemistry Development, Inc).

^h Fitted in our model.

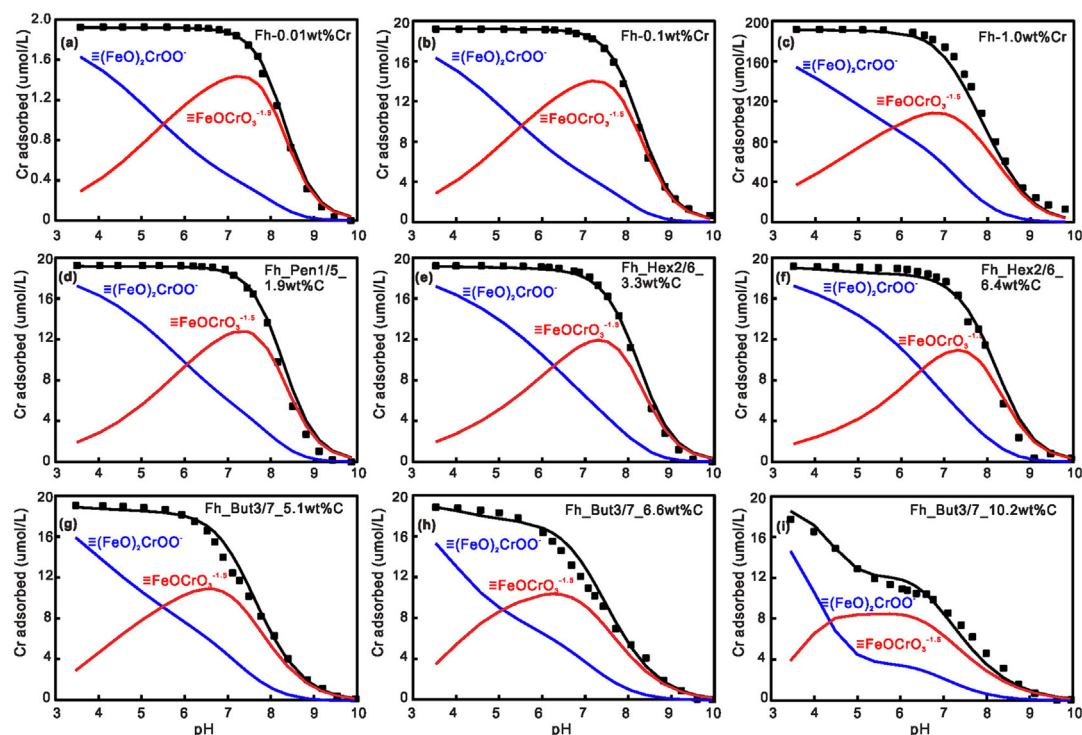


Fig. 2. Model fits for Cr(VI) adsorption on Fh and Fh organominerals. (a)–(c) for pure Fh with Cr(VI) concentrations at 0.01 wt%Cr, 0.1 wt%Cr and 1.0 wt%Cr at 100% adsorption (1.92×10^{-6} , 1.92×10^{-5} , 1.92×10^{-4} M [Cr(VI)_{total}], respectively). (d)–(i) for Fh organominerals with Cr(VI) concentration at 0.1 wt%Cr at 100% adsorption (1.92×10^{-5} M [Cr(VI)_{total}]). Black solid squares are the Cr(VI) adsorption experimental data; black lines are the predicted total Cr(VI) adsorption; blue lines are the predicted bidentate Cr(VI) complexes ($\equiv(\text{FeO})_2\text{CrOO}^-$); red lines are the predicted monodentate Cr(VI) complexes ($\equiv\text{FeOCrO}_3^{-1.5}$). Pen1/5, Hex2/6 and But3/7 represent simple carboxyl-rich OC with one-, two- and three-carboxyl groups, respectively. (For interpretation of the references to colour in this figure legend, the reader is referred to the web version of this article.)

aging at pH 5 and 6.5, but the final proportion of Cr(VI)_{strongly-bound} at pH 6.5 is lower than that at pH 5.0 (Fig. 3). A similar phenomenon is also observed in which the final proportion of Cr(VI)_{strongly-bound} at pH 7.0 is much lower than at pH 5.0 during the aging of Cr(VI)–Fh coprecipitates (Yu et al., 2021). This might be attributed to a faster aging rate at pH 6.5 (Fig. S2b, c) and thus a reduced time for Cr(VI) to penetrate inside Fe minerals. This might also be attributed to the different binding strengths of monodentate and bidentate Cr(VI) complexes. It is reported that Se(IV) that is strongly-bound to Fh via inner-sphere complexation is more easily captured into neoformed Fe minerals during aging of Fh than Se(IV) that is weakly-bound via outer-sphere complexation (Börsig et al., 2017). In our experiment, the strongly-bound bidentate Cr(VI) complex dominates at pH 5.0, while the weakly-bound monodentate Cr(VI) complex dominates at pH 6.5. During aging at pH 6.5, it is therefore likely that the lower proportion of bidentate Cr(VI) complexes results in less Cr(VI) incorporated into Fe minerals formed after aging.

4.2.2. Redistribution of Cr(VI) in Fh organomineral systems

4.2.2.1. Redistribution of Cr(VI) for Fh_Pen1/5 coprecipitates. The presence of OC can influence Cr(VI) retained during aging of Fh organominerals in a number of different ways, namely via influencing Cr(VI) adsorption, influencing the properties of Fe minerals formed after aging and retarding the aging rate of Fh.

For Fh_Pen1/5_1.2 wt%C with 0.1 wt%Cr at 100% adsorption, essentially all Cr(VI) is associated with solid minerals during aging, and $\sim 100\%$ of the solid-associated Cr(VI) is strongly-bound after 19 days aging (Fig. 4), which is significantly higher compared to pure Fh with equivalent Cr(VI) (Fig. 3). The rate constant for Cr(VI) retained ($b = 0.634 \pm 0.077$) is nearly twice that for pure Fh ($b = 0.337 \pm 0.023$) at pH 5.0, and also higher than that for pure Fh at pH 6.5 (Table 3).

The effect of Pen1/5 on Cr(VI) retained however, is unlikely to be due to a direct influence on Cr(VI) adsorption. Essentially the presence of Pen1/5 results in no discernable decrease in the adsorption of Cr(VI) (Fig. 1), and actually, previous work shows that Fh organominerals made with weakly-bound OC like Pen1/5 show a faster adsorption of As(V) and desorption of the weakly-bound OC facilitates As(V) uptake (Mikutta et al., 2014). As such a similar situation may occur here, more strongly-bound Cr(VI) should readily replace weakly-bound Pen1/5 to access adsorption sites if Fe minerals formed after aging cannot host all of the OC and Cr(VI), as the SSA of Fe minerals decreases significantly during aging. The favourable access of Cr(VI) to adsorption sites then likely facilitates its retention within Fe minerals. Similarly, whilst the presence of Pen1/5 retards the aging of Fh, the Cr(VI) retained during aging is not delayed compared to the pure Fh system (Table 3). The effect of Pen1/5 on the distribution of Cr is therefore instead attributed to the way that OC influences the properties of Fe minerals, namely resulting in larger SSA and TPV of Fe minerals than those formed from pure Fh after aging. The surface pores in Fh can promote the adsorption of As(V) and inhibit the desorption of As(V) (Mikutta et al., 2014). As such, the porous structure of Fe minerals likely favours the retention of Cr(VI) within Fe minerals during aging, and thus leads to more Cr(VI)_{strongly-bound} (Fig. 4) and a higher rate constant for Cr(VI) retained compared to the pure Fh system.

4.2.2.2. Redistribution of Cr(VI) for Fh_Hex2/6 organominerals. For Fh_Hex2/6 organominerals, again essentially all Cr(VI) is associated with solid minerals during aging, and $>90\%$ of the solid-associated Cr(VI) is strongly-bound after 19 days aging (Fig. 4), which is significantly higher compared to pure Fh with equivalent Cr(VI) (Fig. 3). The rate constants for the capture of Cr(VI) ($b = 0.555 \pm 0.004/0.461 \pm 0.041$) are higher than that for pure Fh ($b = 0.$

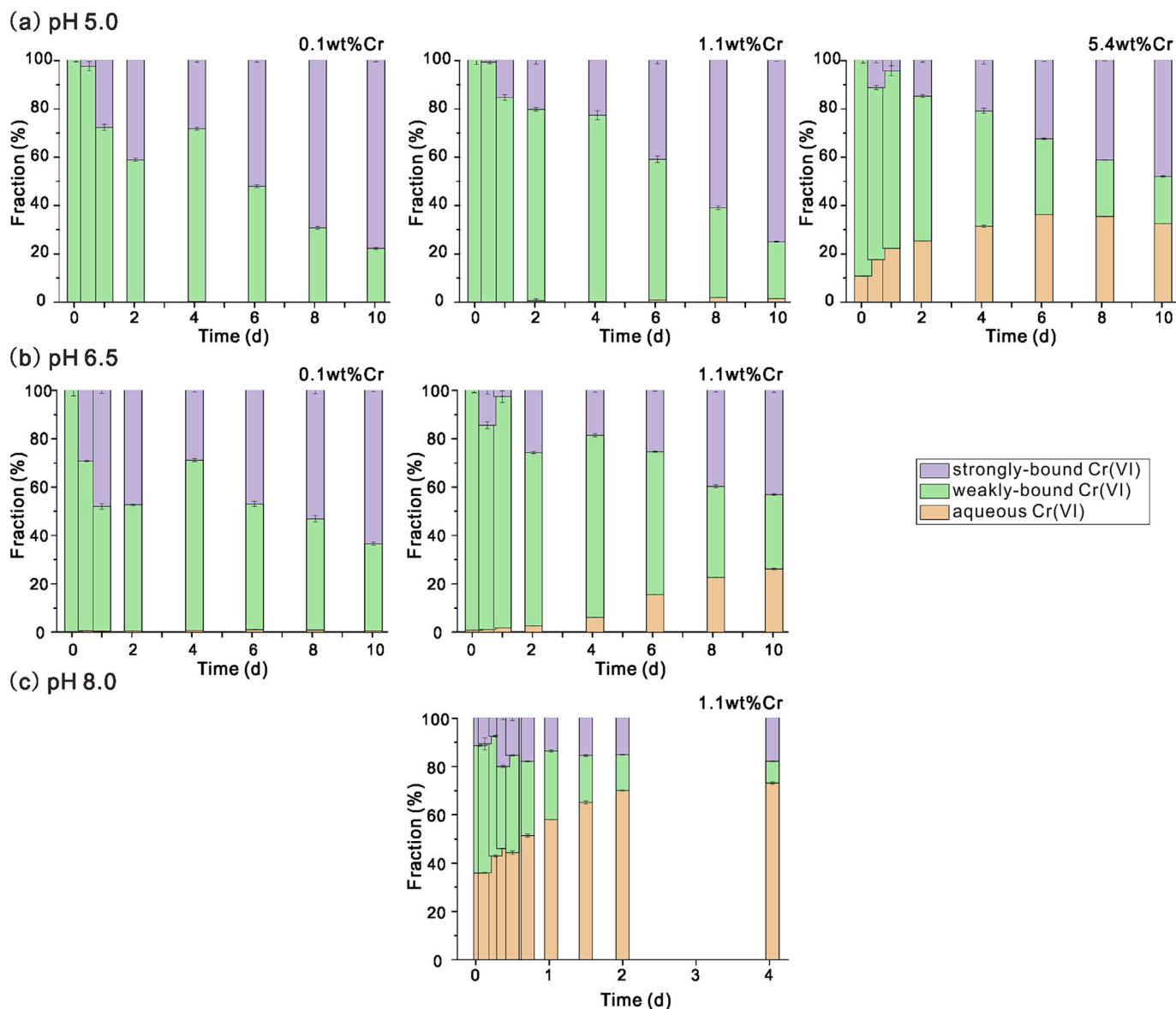


Fig. 3. Distribution of Cr(VI) with different Cr(VI) adsorbed (0.1 wt%Cr, 1.1 wt%Cr and 5.4 wt%Cr at 100% adsorption) during aging of Fh at pH 5, pH 6.5 and pH 8. Error bars represent standard deviations of at least duplicate samples.

337 ± 0.023) at pH 5.0, but are much reduced and similar to pure Fh ($b = 0.418 \pm 0.001/0.279 \pm 0.015$ for Fh_Hex2/6 composites vs. $b = 0.351 \pm 0.113$ for pure Fh) as pH increases to 6.5 (Table 3).

As for Pen1/5, the effect of Hex2/6 on Cr(VI) retained is unlikely to be due to a direct influence on Cr(VI) adsorption. Whilst the presence of Hex2/6 results in a minor decrease in the adsorption of Cr(VI), this is negligible at or below pH 6.5 (Fig. 1). Again as for Pen1/5, despite the retardation of Hex2/6 on the aging of Fh, Cr(VI) retained during aging is not delayed compared to the pure Fh system (Table 3). The effect of Hex2/6 on Cr(VI) retained is therefore also attributed to the porous structure of Fe minerals caused by the presence of OC, which thus leads to the higher final proportion of Cr(VI)_{strongly-bound} (Fig. 4) and the higher rate constant for Cr(VI) retained (Table 3) compared to the pure Fh system.

It is notable that Fh_Hex2/6 organominerals have much higher rate constants for Cr(VI) retained at pH 5, but similar rate constants to pure Fh at pH 6.5. This is possibly an indirect consequence of the influence of Hex2/6 on Cr(VI) adsorption at different pH conditions. During aging, the total C% for Fh_Hex2/6 organominerals decreases

(Fig. S4), and this suggests that the Fe minerals may have an over-saturated surface coverage with respect to OC, such that they cannot host all the OC during aging. At pH 5.0, Hex2/6 is adsorbed via two- and one-carboxyl binding, with similar or smaller binding strengths compared to the dominating bidentate Cr(VI) complex; but at pH 6.5, Hex2/6 is also adsorbed via two- and one-carboxyl binding, but with stronger or similar binding strengths compared to the dominating monodentate Cr(VI) complex (Fig. 2). Thus at pH 5, bidentate Cr(VI) more easily replaces Hex2/6 and is thus more easily retained inside Fe minerals, resulting in much higher rate constants for Cr(VI) retained compared to pure Fh, while at pH 6.5, monodentate Cr(VI) less easily replaces Hex2/6 and is thus less easily retained inside Fe minerals, resulting in similar rate constants for Cr(VI) retained compared to pure Fh.

4.2.2.3. Redistribution of Cr(VI) for Fh_But3/7 organominerals. Differing from Fh_Pen1/5 and Fh_Hex2/6 organominerals, for Fh_But3/7 organominerals not all Cr(VI) is associated with the solid minerals, such that there is significant aqueous Cr(VI)

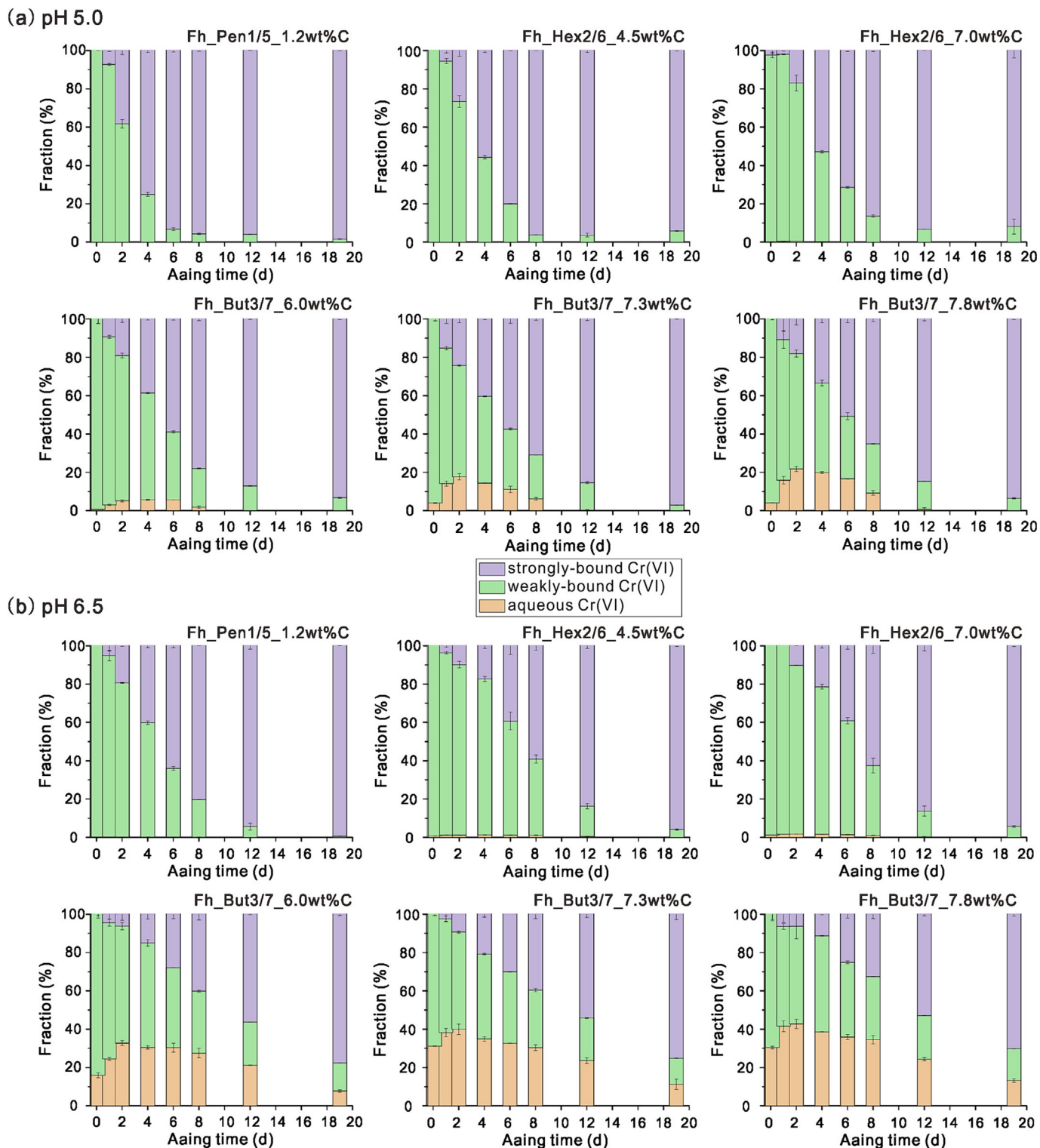


Fig. 4. Distribution of Cr(VI) with 0.1 wt%Cr at 100% adsorption during the aging of Fh organominerals at (a) pH 5 and (b) 6.5. Error bars represent standard deviations of at least duplicate samples.

released during aging. After 19 days aging up to ~10% of the total Cr(VI) is aqueous Cr(VI), while ~70–~90% of the solid-associated Cr(VI) is strongly-bound (Fig. 4). The fraction of Cr(VI)_{strongly-bound} however, is still significantly higher than that for pure Fh (Fig. 3). The rate constants for Cr(VI) retained ($b = 0.406 \pm 0.001/0.352 \pm 0.022/0.305 \pm 0.009$) are higher or equivalent to that for pure Fh ($b = 0.337 \pm 0.023$) at pH 5.0, but are much reduced and lower than that

for pure Fh ($b = 0.191 \pm 0.004/0.189 \pm 0.012/0.148 \pm 0.009$ for Fh_But3/7 composites vs. $b = 0.351 \pm 0.113$ for pure Fh) as pH increases to 6.5 (Table 3). Notably there is an increase in aqueous Cr(VI) during the initial stages of aging, which then decreases as the aging proceeds, where aqueous Cr(VI) also increases with the C loading of the organominerals (Fig. 4). We attribute the effect of But3/7 on the distribution of Cr(VI) to a combination of a direct

Table 3
Rates of Cr(VI) retained during aging of Fh and Fh organominerals.

	pH 5			pH 6.5		
	a	b (h ⁻¹)	R ²	a	b (h ⁻¹)	R ²
Pure Fh	0	0.337 ± 0.023	0.96	0	0.351 ± 0.113	0.52
Fh_Pen1/5_1.2 wt%C	0	0.634 ± 0.077	0.93	0	0.418 ± 0.001	1.00
Fh_Hex2/6_4.5 wt%C	0	0.555 ± 0.004	1.00	0	0.279 ± 0.015	0.98
Fh_Hex2/6_7.0 wt%C	0	0.461 ± 0.041	0.96	-4.5	0.308 ± 0.016	0.98
Fh_But3/7_6.0 wt%C	0	0.406 ± 0.001	1.00	0	0.191 ± 0.004	1.00
Fh_But3/7_7.3 wt%C	0	0.352 ± 0.022	0.97	2.59	0.189 ± 0.012	0.97
Fh_But3/7_7.8 wt%C	0	0.305 ± 0.009	0.99	0	0.148 ± 0.009	0.97

The increasing proportions of Cr(VI)_{strongly-bound} (from 0 to ~80%) with aging time are fitted with the rate equation: $[A]_t = a + b \times t$, where a is intercept of the linear fit, and b is the slope of the linear fit, representing the rate of Cr(VI) retained (i.e., redistribution of Cr(VI) from the weakly-bound to strongly-bound fraction).

Table 4
Surface coverage of Fh fraction of different organominerals by organic acids and Cr(VI).

Organo-minerals ^a	Organic matter (wt%)	Mineral wt%	Total surface sites of Fh (mmol) ^b	Cr(VI) (mmol)	Coverage of Fh by Cr(VI) bidentate complex (%)	Total carboxyl groups (mmol)	Coverage of Fh with one carboxyl adsorbed (%)	Coverage of Fh with two carboxyl adsorbed (%)	Coverage of Fh with three carboxyl adsorbed (%)
Fh_Pen1/			5_1.9 wt% C	3.23	96.77	0.08680	0.00058	1.34	0.00949
10.93 Fh_Hex2/			6_3.3 wt% C	6.69	93.31	0.08370	0.00058	1.38	0.02748
32.84 Fh_Hex2/			6_6.4 wt% C	12.97	87.03	0.07807	0.00058	1.48	0.05329
16.42 Fh_But3/			7_5.1 wt% C	11.53	88.47	0.07936	0.00058	1.45	0.05460
45.87 Fh_But3/	68.8		7_6.6 wt% C	14.92	85.08	0.07632	0.00058	1.51	0.07066
61.72 Fh_But3/	92.58		7_10.2 wt% C	23.05	76.95	0.06902	0.00058	1.67	0.10919
105.47	158.20								

^a Fixed at 0.03 g for further calculation because the suspension for all systems is 30 mL with 1 g dry sorbent L⁻¹.

^b Estimated from calculation using the surface site density of pure Fh weighted to the mineral:OC mass ratio of each organomineral (Table 2).

influence on Cr(VI) adsorption, an influence on the properties of Fe minerals and an influence on the aging rate.

Regarding the change in aqueous Cr(VI), But3/7 causes a strong suppression of Cr(VI) adsorption onto Fh_But3/7 organominerals (Fig. 1). During aging of Fh organominerals, the SSA of Fe minerals decreases, whilst But3/7 leads to a porous structure of Fe minerals. Taken together, the inhibition effects of But3/7 on Cr(VI) adsorption becomes more pronounced as the SSA and thus the adsorption capacity of Fe minerals decrease with the aging process in the first several days, leading to higher proportions of aqueous Cr(VI) (Fig. 4). The inhibition effects on Cr(VI) adsorption are alleviated as the aging further proceeds however, by enhanced release of OC from the mineral surface with decreasing SSA (Fig. S4), and a substantially slowed aging rate (Fig. S3), which together makes more surface sites available, and provides more time, for the smaller sized Cr(VI) to be re-adsorbed. After 19 days aging, the final fraction of aqueous Cr(VI) is even lower than that before the aging of Fh organominerals at pH 6.5, suggesting that the aging of Fe (oxyhydr)oxide eventually decreases the mobility of Cr(VI) although the fraction of aqueous Cr(VI) indeed increases during aging.

Regarding Cr(VI) retained, the total C% for Fh_But3/7 organominerals decreases during aging (Fig. S4), and in addition, the initial Fh_But3/7 organominerals have an oversaturated sur-

face coverage with respect to OC (Table 4), such that Fe minerals formed after aging with lower SSA certainly have an oversaturated surface coverage with respect to OC, and are unlikely to be able to host all the OC. At pH 5.0, But3/7 is adsorbed via three- or two-carboxyl binding with stronger or similar binding strengths compared to the dominating bidentate Cr(VI) complex; but at pH 6.5, But3/7 is also adsorbed via three- and two-carboxyl binding, but with much stronger binding strengths compared to the dominating monodentate Cr(VI) complex (Fig. 2). Thus at pH 5, whilst bidentate Cr(VI) cannot easily replace But3/7, it can more easily replace But3/7 than monodentate Cr(VI) at pH 6.5; and in addition, the porous structure of Fe minerals favours the retention of Cr(VI). Taken together these effects result in slightly higher or equivalent rate constants for Cr(VI) retained at pH 5.0 compared to pure Fh, because the effects of bidentate Cr(VI) and a more porous mineral structure positively combine; but much lower rate constants at pH 6.5 compared to pure Fh, where the effects of monodentate Cr(VI) and substantially slower aging rate negatively combine to result in slower overall Cr(VI) retained. On the whole, for Fh_But3/7 organominerals however, the fraction of Cr(VI)_{strongly-bound} after 19 days aging is still slightly higher at pH 5.0 (~90% vs. ~80% for equivalent pure Fh) and pH 6.5 (~70% vs. ~65% for equivalent pure Fh) compared to pure Fh (Figs. 3 and 4).

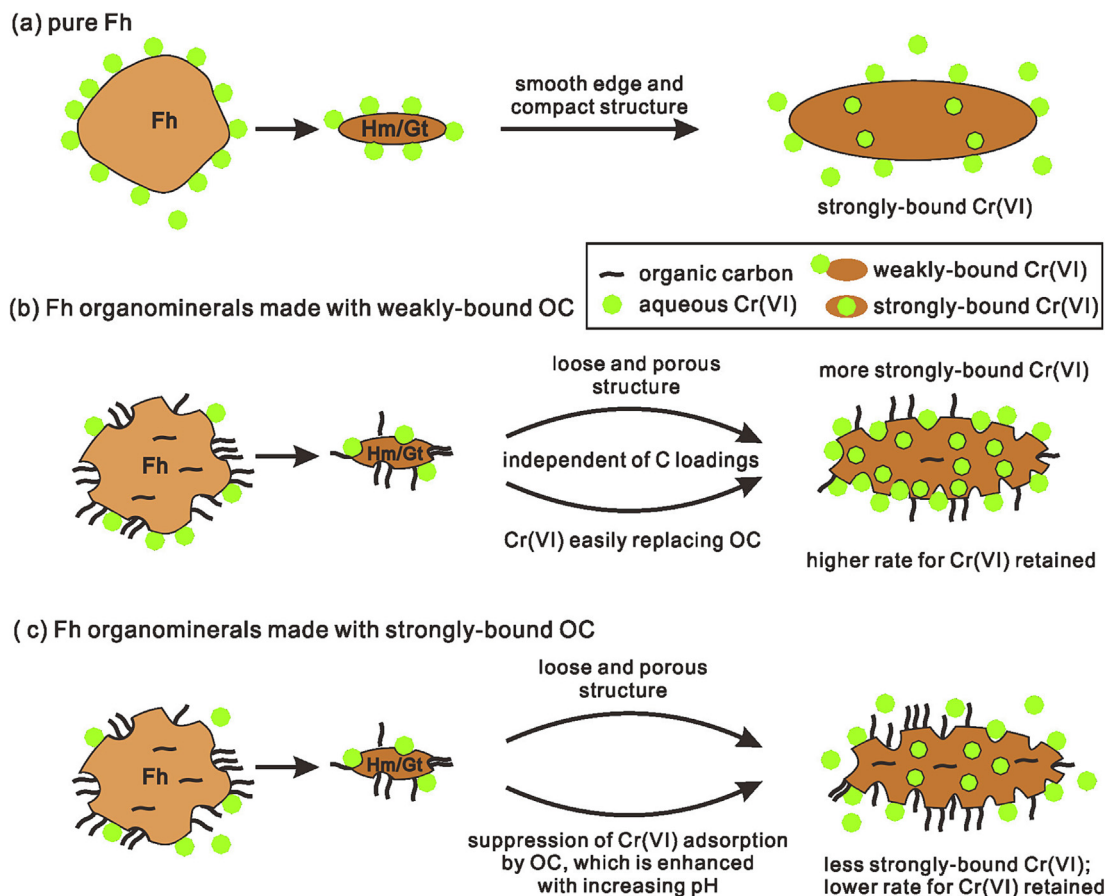


Fig. 5. Diagram illustrating the influence of OC with different binding strengths on the total amount of $\text{Cr(VI)}_{\text{strongly-bound}}$ and the rate constant for Cr(VI) retained inside structural defects and surface pores of Fe minerals during aging of Fh organominerals.

4.2.2.4. Summary of the influence of OC on Cr(VI) redistribution. Overall the redistribution of Cr(VI) during aging of Fh organominerals is strongly controlled by the effects of OC on the properties of Fe minerals, where the presence of OC results in a loose and porous structure of Fe minerals formed after aging, which significantly increases the final proportion of $\text{Cr(VI)}_{\text{strongly-bound}}$ compared to pure Fh (Fig. 5a). The redistribution of Cr(VI) is also influenced by the effects of OC on Cr(VI) adsorption, and specifically the relative binding strength of OC and Cr(VI) . Weakly-bound carboxyl-poor OC has negligible influence on Cr(VI) adsorption because Cr(VI) can easily replace OC to access adsorption sites and surface pores, which increases the rate constant for Cr(VI) retained and increases the final proportion of $\text{Cr(VI)}_{\text{strongly-bound}}$, compared to pure Fh system (Fig. 5b). Strongly-bound carboxyl-rich OC however, significantly inhibits Cr(VI) adsorption, which results in lower rate constants for Cr(VI) retained and lower proportion of $\text{Cr(VI)}_{\text{strongly-bound}}$ compared to carboxyl-poor organominerals, and lower rate constants for Cr(VI) retained at higher pH compared to pure Fh (Fig. 5c). Based on our results however, increasingly strongly-bound carboxyl-rich OC and elevated C loadings with Fe (oxyhydr)oxides may result in lower rate constants for Cr(VI) retained and lower proportions of $\text{Cr(VI)}_{\text{strongly-bound}}$ after aging compared to pure Fh.

4.3. Environmental importance

This study demonstrates the importance of relative binding strength between OC and Cr(VI) in controlling the mobility and fate of Cr(VI) during aging of Fh organominerals, which provides a new

insight into the role of different additives, like OC, in controlling the cycling of Cr in geochemical systems. Our results indicate that in contaminated soils, the carboxyl-richness of OC might be used as a factor to estimate the environmental risk of Cr(VI) , because we predict that Cr(VI) has higher mobility in the presence of carboxyl-rich OC like humic acid and may pose a greater hazard to plants and animals. Meanwhile, our results indicate that in contaminated soils, Cr(VI) may be effectively fixed with Fh organominerals made with weakly-bound OC, such that this material might be used as part of a successful remediation approach. Overall, our work provides new information about the fundamental mechanisms responsible for Cr(VI) mobility and fate in geochemical systems, which might be used as a mechanistic platform to develop remediation approaches for Cr(VI) in contaminated soils.

5. Conclusion

Our adsorption experiment and surface complexation model results show that the binding strengths of carboxylic OC and Cr(VI) complexes follow the order one-carboxyl OC binding \sim monodentate Cr(VI) binding $<$ two carboxyl OC binding \sim bidentate Cr(VI) binding $<$ three-carboxyl OC binding. Regarding the influence of OC with different binding strengths on Cr(VI) adsorption, for Fh_Pen1/5 and Fh_Hex2/6 organominerals, the presence of weakly bound OC at different C loadings has almost no discernible influence on Cr(VI) adsorption, while for Fh_But3/7 organominerals, the more strongly bound OC significantly suppresses Cr(VI) adsorption via surface site blocking and/or electrostatic repulsion. Regarding the Cr(VI) redistribution during aging,

for pure Fh we show that the fraction of aqueous Cr(VI) increases with aging time, and is enhanced with increasing Cr(VI) concentrations and pH, whilst the fraction of Cr(VI)_{strongly-bound} increases with aging time. For Fh organominerals, the mobility and fate of Cr(VI) is strongly controlled by how OC affects the properties of Fe minerals. In particular the loose and porous structure of the Fe minerals caused by OC significantly increases the final proportion of Cr(VI)_{strongly-bound}. The mobility and fate of Cr(VI) is also influenced by how OC affects Cr(VI) adsorption, and specifically the relative binding strength of OC and Cr(VI): weakly-bound carboxyl-poor OC has negligible influence on Cr(VI) adsorption because Cr(VI) can easily replace OC to access adsorption sites, and together with the loose and porous structure of Fe minerals, this increases the rate of Cr(VI) retained and increases the final proportion of Cr(VI)_{strongly-bound}; strongly-bound carboxyl-rich OC however, significantly inhibits Cr(VI) adsorption, which results in lower rate constants for Cr(VI) retained and decreases the final proportion of Cr(VI)_{strongly-bound}, compared to carboxyl-poor organominerals. The mobility and fate of Cr(VI) in soils and sediments as Fh organominerals age is therefore likely strongly controlled by the carboxyl-richness of OC in the organominerals. A further study focused on the molecular bonding environment of Cr(VI) retained in Fe minerals is suggested, as molecular level information should reveal the precise mechanisms in operation during the Cr(VI) retention process and shed further light on the retention or release of Cr(VI) during aging of Fe (oxyhydr)oxides.

Declaration of Competing Interest

The authors declare that they have no known competing financial interests or personal relationships that could have appeared to influence the work reported in this paper.

Acknowledgement

We thank laboratory managers Andrew Hobson and Stephen Reid, and laboratory technician Fiona Keay (University of Leeds) for laboratory support. A. O. F. and C. L. P. gratefully acknowledge NERC Highlight Topic Grant (NE/S004963/1 Locked Up). Y. Z. gratefully acknowledges support from the China Scholarship Council. C. L. P. gratefully acknowledges Royal Society Wolfson Research Merit Award (WRM/FT/170005).

Appendix A. Supplementary material

Supplementary file associated with this article can be found in the online version, mainly including physiochemical characteristics of Fe (oxyhydr)oxide by acid-leaching method during aging, aqueous chromium speciation, redistribution of OC and model fitting to increasing proportions of Cr(VI)_{strongly-bound} during aging. Supplementary material to this article can be found online at <https://doi.org/10.1016/j.gca.2023.02.021>.

References:

Barcelona, M., 1980. Dissolved organic carbon and volatile fatty acids in marine sediment pore waters. *Geochim. Cosmochim. Acta* 44, 1977–1984.
 Barnhart, J., 1997. Occurrences, Uses, and Properties of Chromium. *Regul. Toxicol. Pharm.* 26, S3–S7.
 Bompoti, N.M., Chrysochoou, M., Machesky, M.L., 2019. A Unified Surface Complexation Modeling Approach for Chromate Adsorption on Iron Oxides. *Environ. Sci. Technol.* 53, 6352–6361.
 Börsig, N., Scheinost, A.C., Shaw, S., Schild, D., Neumann, T., 2017. Uptake mechanisms of selenium oxyanions during the ferrihydrite-hematite recrystallization. *Geochim. Cosmochim. Acta* 206, 236–253.
 Chandra, P., Kulshreshtha, K., 2004. Chromium accumulation and toxicity in aquatic vascular plants. *Bot. Rev.* 70, 313–327.

Charlton, S.R., Parkhurst, D.L., 2002. PHREEQCI—A graphical user interface to the geochemical model PHREEQC. US Geological Survey Fact Sheet FS-0311-02.
 Chen, C., Dynes, J.J., Wang, J., Sparks, D.L., 2014. Properties of Fe-Organic Matter Associations via Coprecipitation versus Adsorption. *Environ. Sci. Technol.* 48, 13751–13759.
 Cornell, R.M., Schwertmann, U., 2003. The iron oxides: structure, properties, reactions, occurrences and uses. VCH, Weinheim.
 Costa, M., 1997. Toxicity and Carcinogenicity of Cr(VI) in Animal Models and Humans. *Crit. Rev. Toxicol.* 27, 431–442.
 Curti, L., Moore, O.W., Babakhani, P., Xiao, K.-Q., Wouds, C., Bray, A.W., Fisher, B.J., Kazemian, M., Kaulich, B., Peacock, C.L., 2021. Carboxyl-richness controls organic carbon preservation during coprecipitation with iron (oxyhydr)oxides in the natural environment. *Commun. Earth Environ.* 2, 229.
 Darrie, G., 2001. Commercial Extraction Technology and Process Waste Disposal in the Manufacture of Chromium chemicals From Ore. *Environ. Geochem. Health* 23, 187–193.
 Das, S., Hendry, M.J., Essilfie-Dughan, J., 2011. Transformation of Two-Line Ferrihydrite to Goethite and Hematite as a Function of pH and Temperature. *Environ. Sci. Technol.* 45, 268–275.
 Dean, J.A., 1987. *Handbook of Organic Chemistry*. McGraw-Hill Book Co., New York, NY.
 Ding, Z., Fu, F., Dionysiou, D.D., Tang, B., 2018. Coadsorption and subsequent redox conversion behaviors of As(III) and Cr(VI) on Al-containing ferrihydrite. *Environ. Pollut.* 235, 660–669.
 Eusterhues, K., Wagner, F.E., Häusler, W., Hanzlik, M., Knicker, H., Totsche, K.U., Kögel-Knabner, I., Schwertmann, U., 2008. Characterization of Ferrihydrite-Soil Organic Matter Coprecipitates by X-ray Diffraction and Mössbauer Spectroscopy. *Environ. Sci. Technol.* 42, 7891–7897.
 Eusterhues, K., Rennert, T., Knicker, H., Kögel-Knabner, I., Totsche, K.U., Schwertmann, U., 2011. Fractionation of Organic Matter Due to Reaction with Ferrihydrite: Coprecipitation versus Adsorption. *Environ. Sci. Technol.* 45, 527–533.
 Eusterhues, K., Hädrich, A., Neidhardt, J., Küsel, K., Keller, T.F., Jandt, K.D., Totsche, K. U., 2014. Reduction of ferrihydrite with adsorbed and coprecipitated organic matter: microbial reduction by *Geobacter bremsensis* vs. abiotic reduction by Na-dithionite. *BIOGEOSCIENCES* 11, 4953–4966.
 Evanko, C.R., Dzombak, D.A., 1999. Surface Complexation Modeling of Organic Acid Sorption to Goethite. *J. Colloid Interface Sci.* 214, 189–206.
 Fendorf, S., Eick, M.J., Grossl, P., Sparks, D.L., 1997. Arsenate and Chromate Retention Mechanisms on Goethite. 1. Surface Structure. *Environ. Sci. Technol.* 31, 315–320.
 Field, H.R., Whitaker, A.H., Henson, J.A., Duckworth, O.W., 2019. Sorption of copper and phosphate to diverse biogenic iron (oxyhydr)oxide deposits. *Sci. Total Environ.* 697, 134111.
 Francisco, P.C.M., Sato, T., Otake, T., Kasama, T., Suzuki, S., Shiwaku, H., Yaita, T., 2018. Mechanisms of Se(IV) Co-precipitation with Ferrihydrite at Acidic and Alkaline Conditions and Its Behavior during Aging. *Environ. Sci. Technol.* 52, 4817–4826.
 Grossl, P.R., Eick, M., Sparks, D.L., Goldberg, S., Ainsworth, C.C., 1997. Arsenate and Chromate Retention Mechanisms on Goethite. 2. Kinetic Evaluation Using a Pressure-Jump Relaxation Technique. *Environ. Sci. Technol.* 31, 321–326.
 Gu, B., Schmitt, J., Chen, Z., Liang, L., McCarthy, J.F., 1995. Adsorption and desorption of different organic matter fractions on iron oxide. *Geochim. Cosmochim. Acta* 59, 219–229.
 Gu, X., Xie, J., Wang, X., Evans, L.J., 2017. A simple model to predict chromate partitioning in selected soils from China. *J. Hazard. Mater.* 322, 421–429.
 Hajji, S., Montes-Hernandez, G., Sarret, G., Tordo, A., Morin, G., Ona-Nguema, G., Bureau, S., Turki, T., Mzoughi, N., 2019. Arsenite and chromate sequestration onto ferrihydrite, siderite and goethite nanostructured minerals: Isotherms from flow-through reactor experiments and XAS measurements. *J. Hazard. Mater.* 362, 358–367.
 Hiemstra, T., 2013. Surface and mineral structure of ferrihydrite. *Geochim. Cosmochim. Acta* 105, 316–325.
 Hiemstra, T., Van Riemsdijk, W.H., 2009. A surface structural model for ferrihydrite I: Sites related to primary charge, molar mass, and mass density. *Geochim. Cosmochim. Acta* 73, 4423–4436.
 Hiemstra, T., Van Riemsdijk, W.H., Bolt, G.H., 1989. Multisite proton adsorption modeling at the solid/solution interface of (hydr)oxides: A new approach: I. Model description and evaluation of intrinsic reaction constants. *J. Colloid Interface Sci.* 133, 91–104.
 Hiemstra, T., Venema, P., Riemsdijk, W.H.V., 1996. Intrinsic Proton Affinity of Reactive Surface Groups of Metal (Hydr)oxides: The Bond Valence Principle. *J. Colloid Interface Sci.* 184, 680–692.
 Hu, S., Lu, Y., Peng, L., Wang, P., Zhu, M., Dohnalkova, A.C., Chen, H., Lin, Z., Dang, Z., Shi, Z., 2018. Coupled Kinetics of Ferrihydrite Transformation and As(V) Sequestration under the Effect of Humic Acids: A Mechanistic and Quantitative Study. *Environ. Sci. Technol.* 52, 11632–11641.
 Hu, S., Liang, Y., Liu, T., Li, F., Lu, Y., Shi, Z., 2020. Kinetics of As(V) and carbon sequestration during Fe(II)-induced transformation of ferrihydrite-As(V)-fulvic acid coprecipitates. *Geochim. Cosmochim. Acta* 272, 160–176.
 Jacobs, J.A., Testa, S.M., 2005. Overview of chromium (VI) in the environment: background and history. *Chromium Handbook*, 1–21.
 Johnston, C.P., Chrysochoou, M., 2012. Investigation of Chromate Coordination on Ferrihydrite by In Situ ATR-FTIR Spectroscopy and Theoretical Frequency Calculations. *Environ. Sci. Technol.* 46, 5851–5858.

- Johnston, C.P., Chrysochoou, M., 2014. Mechanisms of chromate adsorption on hematite. *Geochim. Cosmochim. Acta* 138, 146–157.
- Johnston, C.P., Chrysochoou, M., 2016. Mechanisms of Chromate, Selenate, and Sulfate Adsorption on Al-Substituted Ferrihydrite: Implications for Ferrihydrite Surface Structure and Reactivity. *Environ. Sci. Technol.* 50, 3589–3596.
- Jones, D., 1998. Organic Acids in the Rhizosphere - a Critical Review. *Plant Soil* 205, 23–44.
- Larsen, O., Postma, D., 2001. Kinetics of reductive bulk dissolution of lepidocrocite, ferrihydrite, and goethite. *Geochim. Cosmochim. Acta* 65, 1367–1379.
- Lehmann, J., Skjemstad, J., Sohi, S., Carter, J., Michele, B., Falloon, P., Coleman, K., Woodbury, P., Krull, E., 2008. Australian climate-carbon feedback reduced by soil black carbon. *Nat. Geosci.* 1.
- Lv, J., Zhang, S., Wang, S., Luo, L., Cao, D., Christie, P., 2016. Molecular-Scale Investigation with ESI-FT-ICR-MS on Fractionation of Dissolved Organic Matter Induced by Adsorption on Iron Oxyhydroxides. *Environ. Sci. Technol.* 50, 2328–2336.
- Mesuer, K., Fish, W., 1992a. Chromate and oxalate adsorption on goethite. 1. Calibration of surface complexation models. *Environ. Sci. Technol.* 26, 2357–2364.
- Mesuer, K., Fish, W., 1992b. Chromate and oxalate adsorption on goethite. 2. Surface complexation modeling of competitive adsorption. *Environ. Sci. Technol.* 26, 2365–2370.
- Michel, F.M., Ehm, L., Liu, G., Han, W.Q., Antao, S.M., Chupas, P.J., Lee, P.L., Knorr, K., Eulert, H., Kim, J., Grey, C.P., Celestian, A.J., Gillow, J., Schoonen, M.A.A., Strongin, D.R., Parise, J.B., 2007. Similarities in 2- and 6-Line Ferrihydrite Based on Pair Distribution Function Analysis of X-ray Total Scattering. *Chem. Mater.* 19, 1489–1496.
- Mikutta, R., Lorenz, D., Guggenberger, G., Haumaier, L., Freund, A., 2014. Properties and reactivity of Fe-organic matter associations formed by coprecipitation versus adsorption: Clues from arsenate batch adsorption. *Geochim. Cosmochim. Acta* 144, 258–276.
- Moon, E.M., Peacock, C.L., 2012. Adsorption of Cu(II) to ferrihydrite and ferrihydrite-bacteria composites: Importance of the carboxyl group for Cu mobility in natural environments. *Geochim. Cosmochim. Acta* 92, 203–219.
- Moon, E.M., Peacock, C.L., 2013. Modelling Cu(II) adsorption to ferrihydrite and ferrihydrite-bacteria composites: Deviation from additive adsorption in the composite sorption system. *Geochim. Cosmochim. Acta* 104, 148–164.
- Otero-Fariña, A., Fiol, S., Arce, F., Antelo, J., 2017. Effects of natural organic matter on the binding of arsenate and copper onto goethite. *Chem. Geol.* 459, 119–128.
- Park, S., Lee, J.-H., Shin, T.J., Hur, H.-G., Kim, M.G., 2018. Adsorption and Incorporation of Arsenic to Biogenic Lepidocrocite Formed in the Presence of Ferrous Iron during Denitrification by *Paracoccus denitrificans*. *Environ. Sci. Technol.* 52, 9983–9991.
- Parkhurst, D.L., Appelo, C., 1999. User's guide to PHREEQC (Version 2): A computer program for speciation, batch-reaction, one-dimensional transport, and inverse geochemical calculations. *Water-resources Investigations Report* 99, 312.
- Rai, D., Zachara, J.M., Eary, L.E., Girvin, D.C., Moore, D.A., Resch, C.T., Sass, B.M., Schmidt, R.L., 1986. Geochemical behaviour of chromium species. *Interim Report EPRI EA-4544, E.P.R.I., Palo Alto, Calif.*
- Rothe, J., Denecke, M.A., Dardenne, K., 2000. Soft X-Ray Spectromicroscopy Investigation of the Interaction of Aquatic Humic Acid and Clay Colloids. *J. Colloid Interface Sci.* 231, 91–97.
- Rowley, M.C., Grand, S., Verrecchia, É.P., 2017. Calcium-mediated stabilisation of soil organic carbon. *Biogeochemistry* 137, 27–49.
- Sakakibara, M., Tanaka, M., Takahashi, Y., Murakami, T., 2019. Redistribution of Zn during transformation of ferrihydrite: Effects of initial Zn concentration. *Chem. Geol.* 522, 121–134.
- Schwertmann, U., Cornell, R.M., 2000. *Iron Oxides in the Laboratory: Preparation and Characterization*, second completely revised and extended edition. Wiley-VCH, Weinheim, Germany.
- Shanker, A.K., Cervantes, C., Loza-Tavera, H., Avudainayagam, S., 2005. Chromium toxicity in plants. *Environ. Int.* 31, 739–753.
- Sherman, D.M., Peacock, C.L., Hubbard, C.G., 2008. Surface complexation of U(VI) on goethite (α -FeOOH). *Geochim. Cosmochim. Acta* 72, 298–310.
- Shimizu, M., Zhou, J., Schröder, C., Obst, M., Kappler, A., Borch, T., 2013. Dissimilatory Reduction and Transformation of Ferrihydrite-Humic Acid Coprecipitates. *Environ. Sci. Technol.* 47, 13375–13384.
- Solomon, D., Lehmann, J., Kinyangi, J., Liang, B., Schäfer, T., 2005. Carbon K-Edge NEXAFS and FTIR-ATR Spectroscopic Investigation of Organic Carbon Speciation in Soils. *Soil Sci. Soc. Am. J.* 69, 107–119.
- Sposito, G., 2008. *The Chemistry of Soils*. Oxford University Press.
- Sun, G., Fu, F., Yu, G., Yu, P., Tang, B., 2021. Migration behavior of Cr(VI) during the transformation of ferrihydrite-Cr(VI) co-precipitates: The interaction between surfactants and co-precipitates. *Sci. Total. Environ.* 767, 145429.
- Veselská, V., Fajgar, R., Čihalová, S., Bolanz, R.M., Göttlicher, J., Steininger, R., Siddique, J.A., Komárek, M., 2016. Chromate adsorption on selected soil minerals: Surface complexation modeling coupled with spectroscopic investigation. *J. Hazard. Mater.* 318, 433–442.
- Wang, Y., Morin, G., Ona-Nguema, G., Juillot, F., Calas, G., Brown, G.E., 2011. Distinctive Arsenic(V) Trapping Modes by Magnetite Nanoparticles Induced by Different Sorption Processes. *Environ. Sci. Technol.* 45, 7258–7266.
- Weng, L., Van Riemsdijk, W.H., Hiemstra, T., 2009. Effects of Fulvic and Humic Acids on Arsenate Adsorption to Goethite: Experiments and Modeling. *Environ. Sci. Technol.* 43, 7198–7204.
- Westall, J., Hohl, H., 1980. A comparison of electrostatic models for the oxide/solution interface. *Advances in Colloid and Interface Science* 12, 265–294.
- Whitaker, A.H., Pena, J., Amor, M., Duckworth, O.W., 2018. Cr(VI) uptake and reduction by biogenic iron (oxyhydr)oxides. *Environ. Sci. Proc. Impacts* 20, 1056–1068.
- Xie, J., Gu, X., Tong, F., Zhao, Y., Tan, Y., 2015. Surface complexation modeling of Cr(VI) adsorption at the goethite-water interface. *J. Colloid Interface Sci.* 455, 55–62.
- Yu, G., Fu, F., Ye, C., Tang, B., 2020. Behaviors and fate of adsorbed Cr(VI) during Fe(II)-induced transformation of ferrihydrite-humic acid co-precipitates. *J. Hazard. Mater.* 392, 122272.
- Yu, P., Fu, F., Sun, G., Tang, B., 2021. Effects of oxalate and citrate on the behavior and redistribution of Cr(VI) during ferrihydrite-Cr(VI) co-precipitates transformation. *Chemosphere* 266, 128977.
- Zhao, Y., Moore, O.W., Xiao, K.-Q., Curti, L., Fariña, A.O., Banwart, S.A., Peacock, C.L., 2022. The role and fate of organic carbon during aging of ferrihydrite. *Geochim. Cosmochim. Acta* 335, 339–355.
- Zhu, L., Fu, F., Tang, B., 2019. Three-dimensional transfer of Cr(VI) co-precipitated with ferrihydrite containing silicate and its redistribution and retention during aging. *Sci. Total Environ.* 696, 133966.
- Zhu, J., Pigna, M., Cozzolino, V., Caporale, A.G., Violante, A., 2010. Competitive sorption of copper(II), chromium(III) and lead(II) on ferrihydrite and two organomineral complexes. *Geoderma* 159, 409–416.